A possible line-like emission feature at 8 keV in the Seyfert 1.2 UGC 3973

L. C. Gallo,[1] A. C. Fabian,[2] Th. Boller,[1] and W. Pietsch[1]

[1] *Max-Planck-Institut für extraterrestrische Physik, Postfach 1312, 85741 Garching, Germany*
[2] *Institute of Astronomy, University of Cambridge, Madingley Road, Cambridge CB3 0HA*

arXiv:astro-ph/0508229v1 10 Aug 2005

ABSTRACT

Two short X-ray exposures ($< 3600\,\text{s}$ each) of the radio-quiet Seyfert 1.2 galaxy UGC 3973 (Mrk 79) were conducted with *XMM-Newton* as part of an AGN snap-shot survey. In this paper we concentrate on the significance and possible origin of a narrow $8\,\text{keV}$ (rest frame) line-like emission feature detected with the pn instrument during the second observation. Simulations show that the feature is significant at $96.0 - 98.4\%$ confidence, depending on what a priori assumptions are made. The feature cannot be attributed to background contamination and appears to be variable (or transient) since it was not detected in the first observation of UGC 3973 six months earlier. However, a constant feature cannot be completely dismissed, based on the 90% upper-limit on the flux from the first observation. There is some indication that the feature is variable over the duration of the second observation as well. We discuss various models (e.g. Ni emission, recombination edges, outflows, disc lines) which could potentially produce an emission feature at such energies.

Key words: galaxies: active – galaxies: individual: UGC 3973 (Mrk 79) – galaxies: nuclei – X-ray: galaxies

1 INTRODUCTION

UGC 3973 (Mrk 79; $z = 0.022$) is an optically well-studied, radio-quiet (e.g. Ho 2002), Seyfert 1.2 galaxy (e.g. Pietsch et al. 1998). Numerous black hole mass estimates exist (e.g. Wandel et al. 1999; Vestergaard 2002; Peterson et al. 2004) which yield a value of $\sim 6 \times 10^7\,\text{M}_\odot$.

UGC 3973 was observed with *XMM-Newton* (Jansen et al. 2001) at two epochs separated by six months as part of an AGN snap-shot survey, the results of which are presented in Gallo et al. (2005; hereafter G05). These short observations constituted the first analysis of the X-ray spectrum of UGC 3973 above $2\,\text{keV}$. In addition to an iron emission line at $\sim 6.4\,\text{keV}$, which was detected at both epochs, G05 report the detection of a narrow emission feature at $7.99 \pm 0.06\,\text{keV}$ (rest frame) during the second (low-flux) observation. In this paper we elaborate the discussion of this $\sim 8\,\text{keV}$ feature. We have scrutinised the reliability of the detection and discuss physical scenarios which could manifest a line-like feature at such energies.

2 OBSERVATIONS AND DATA REDUCTION

During both observations of UGC 3973 all three EPIC instruments functioned normally. The pn (Strüder et al. 2001) and MOS (MOS1 and MOS2; Turner et al. 2001) cameras were operated in small window mode with the medium filter in place. A summary of the obser-

Table 1. Log of *XMM-Newton* observations of UGC 3973. The date and *XMM-Newton* revolution number when the observation was conducted are given in columns (1) and (2), respectively. The total amount of useful exposure (GTI) is shown in column (4), and the estimated number of $0.3 - 10\,\text{keV}$ source counts is reported in column (5).

| (1) Date year.mm.dd	(2) Rev.	(3) Instrument	(4) Exposure (s)	(5) Counts ($0.3 - 10\,\text{keV}$)
2000.10.09	153	pn	1680	21114
		MOS1	1861	5519
		MOS2	1838	5600
2001.04.26	253	pn	3590	20521
		MOS1	5737	9442
		MOS2	5736	9553

vations is provided in Table 1. Details of the data reduction (which were conducted with `XMM-SAS v6.1.0`) are given in G05.

3 SPECTRAL ANALYSIS

The spectra were grouped such that each bin contained at least 20 counts. Spectral fitting was performed using `XSPEC v11.3.1`

Table 2. The broadband $(0.3 - 10\,\mathrm{keV})$ fits to the pn data of UGC 3973 at each epoch found by G05. The revolution number is given in column (1). In column (2) the fit quality (χ^2_ν/dof) is stated. Columns (3)-(13) are fit parameters and quantities which are measured from the model. Column (3) shows the measured column density at the redshift of UGC 3973 ($10^{20}\,\mathrm{cm}^{-2}$). In column (4) the blackbody temperature is given and in column (5) the power-law photon index. The parameters of an absorption edge: energy and optical depth are given in columns (6) and (7), respectively. The emission line parameters: energy, width, and equivalent width, as measured with a Gaussian profile are given in columns (8), (9), and (10), respectively. The observed $0.3 - 10\,\mathrm{keV}$ flux corrected for Galactic absorption in units of $10^{-12}\,\mathrm{erg\,cm^{-2}\,s^{-1}}$ is reported in column (11). The rest frame $2 - 10\,\mathrm{keV}$ luminosity in units of $10^{43}\,\mathrm{erg\,s^{-1}}$ is given in column (12). In column (13) the luminosity ratio between the blackbody and power-law component (corrected for Galactic and intrinsic absorption) in the $0.3 - 10\,\mathrm{keV}$ band is estimated. Values marked with an f denote fixed parameters.

(1) Rev.	(2) χ^2_ν/dof	(3) $N_{\mathrm{H}z}$	(4) kT (eV)	(5) Γ	(6) E_{edge} (eV)	(7) τ	(8) E_{line} (keV)	(9) σ (eV)	(10) EW (eV)	(11) $F_{0.3-10}$	(12) L_{2-10}	(13) $\frac{L_{bb}}{L_{po}}$
153	0.91/480	< 0.63	122 ± 7	1.85 ± 0.04	–	–	$6.33^{+0.08}_{-0.09}$	1^f	117 ± 15	42.75	2.18	0.13
253	1.00/502	< 0.99	116 ± 7	1.67 ± 0.04	726 ± 15	$0.46^{+0.12}_{-0.08}$	6.45 ± 0.07 7.99 ± 0.06	122^{+68}_{-65} 1^f	216^{+42}_{-27} 161 ± 21	21.78	1.28	0.20
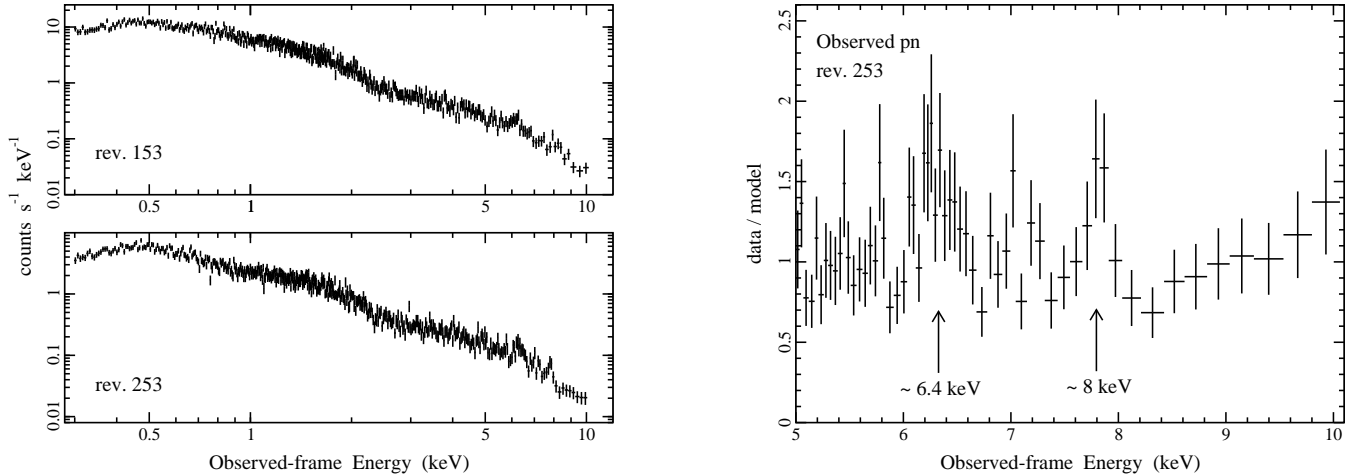
Figure 1. On the left-hand side are the observed $0.3 - 10\,\mathrm{keV}$ count spectra of UGC 3973 during revolution 153 (top panel) and revolution 253 (bottom panel). UGC 3973 was about twice as bright during the first observation. On the right-hand side are the residuals (data/model) remaining in the $5 - 10\,\mathrm{keV}$ range after fitting the broadband spectrum from revolution 153 with a blackbody plus power-law and absorption edge as described in Table 2. Excess residuals at $\sim 6.2\,\mathrm{keV}$ and $\sim 7.8\,\mathrm{keV}$ in the observed frame correspond to $\sim 6.4\,\mathrm{keV}$ and $\sim 8\,\mathrm{keV}$ in the source frame, respectively.

(Arnaud 1996). Fit parameters are reported in the rest frame of the object, although most of the figures remain in the observed frame. The quoted errors on the model parameters correspond to a 90% confidence level for one interesting parameter (i.e. $\Delta\chi^2 = 2.7$ criterion). K-corrected luminosities were derived assuming isotropic emission. A value for the Hubble constant of $H_0 = 70\,\mathrm{km\,s^{-1}\,Mpc^{-1}}$ and a standard cosmology with $\Omega_M = 0.3$ and $\Omega_\Lambda = 0.7$ were adopted. A value for the Galactic column density toward UGC 3973 of $5.69 \times 10^{20}\,\mathrm{cm}^{-2}$ (Dickey & Lockman 1990) was assumed throughout.

3.1 A $7.99\,\mathrm{keV}$ feature

A discussion of the broadband $(0.3-10\,\mathrm{keV})$ and apparent spectral features was presented in G05. In this analysis we assume the best-fitting broadband phenomenological model (Table 2) introduced by G05, and concentrate on the high-energy spectrum. The MOS data

are analysed for consistency, but in the interest of brevity they are discussed only when they appear discordant with the pn data.

During revolution 253 (the second observation) UGC 3973 was about half as bright as it was at the first epoch, and at high-energies it exhibited a flatter spectrum. In addition to neutral (or slightly ionised) iron emission, which was present at both epochs, during revolution 253 a convincing emission-like feature was detected in the rest frame at $7.99 \pm 0.06\,\mathrm{keV}$ ($\sim 7.82\,\mathrm{keV}$ in the observed pn data; Figure 1). When fitted with a Gaussian profile the feature was intrinsically narrow (σ was fixed at $1\,\mathrm{eV}$), and had an equivalent width of $EW = 161 \pm 21\,\mathrm{eV}$ and flux of $f = (1.74 \pm 0.95) \times 10^{-13}\,\mathrm{erg\,cm^{-2}\,s^{-1}}$. The addition of the Gaussian profile improved the existing broadband model by $\Delta\chi^2 = 8.1$ for 2 additional parameters (502 dof). Allowing the width of the Gaussian profile to vary did not improve the fit, nor was the measured value much different than the assumed value of $\sigma = 1\,\mathrm{eV}$.

Attempts to incorporate the $8\,\mathrm{keV}$ and the $\sim 6.4\,\mathrm{keV}$ features

into a single broad line-like profile were unsuccessful. The single broad feature resulted in a poorer fit and large residuals between $6 - 8 \, \mathrm{keV}$.

3.2 Robustness of the detection

3.2.1 *Significance of a physically motivated feature in the $7 - 10 \, \mathrm{keV}$ range*

Given that the feature appears to be transient and that the physical process which created it is unknown, estimating the significance of it is challenging. There are processes which, in principle, could produce emission lines in the $7 - 10 \, \mathrm{keV}$ range, but it is uncertain if they are at work here. As such, we estimate the significance of the feature twice. In this section we assume there is a priori physical motivation to find a line between $7 - 10 \, \mathrm{keV}$ (see Section 4). In the next section we take a more conservative approach and consider the probability of finding such a feature in any spectral channel.

In order to estimate the statistical significance we conducted Monte Carlo simulations similar to the analysis outlined by Porquet et al. (2004). Under the assumption of the broadband spectrum presented in Table 2 (without the Gaussian profile at $7.99 \, \mathrm{keV}$), we simulated 1000 pn spectra mimicking the photon statistics expected from a $3600 \, \mathrm{s}$ exposure. The faked spectra were grouped and fitted in the same manner as the spectrum of UGC 3973. To this model a Gaussian profile with a fixed width of $\sigma = 1 \, \mathrm{eV}$ was added. The two additional free parameters were the line energy, which was limited between $7 - 10 \, \mathrm{keV}$, and the line normalisation. Doing this to the source spectrum resulted in $\Delta \chi^2 = 8.1$. In this manner the $\Delta \chi^2$ was estimated for each of the 1000 fake spectra. In addition, the initial line energy was stepped in $50 \, \mathrm{eV}$ increments between $7 - 10 \, \mathrm{keV}$ and the fit was restarted. The highest $\Delta \chi^2$ was recorded. This step was taken in order to properly sample (oversample) the pn energy resolution, which is $\sim 150 \, \mathrm{eV}$ at $\sim 7 \, \mathrm{keV}$.

A value of $\Delta \chi^2 > 8.1$ was obtained in 16 of the 1000 fake spectra, implying a detection significance of approximately 98.4% confidence for the feature in UGC 3973.

3.2.2 *The "true" significance*

We need to consider the possibility that $\Delta \chi^2 = 8.1$ can be exceeded by a spurious event occuring in any observed energy channel. However, we limit the energy range investigated to $2.3 - 6.4 \, \mathrm{keV}$ and $7.0 - 10.0 \, \mathrm{keV}$. The logic in ignoring the spectrum below $2.3 \, \mathrm{keV}$ is to avoid the calibration uncertainties and astronomical effects (e.g. warm-absorbers in the source or Galaxy) which would affect the observations. We also neglect the $6.4 - 7.0 \, \mathrm{keV}$ range, where an emission feature would be expected.

Following the procedure outlined in the previous section, we find that $\Delta \chi^2 = 8.1$ is exceeded in 20 out of 1000 trials, resulting in a confidence level of 98.0%. Moreover, the overall significance of the observed feature must account for the total number of observations performed (in this case 2). Therefore, by making no assumptions of the physical origin of the feature, the emission-like line at $8 \, \mathrm{keV}$ is detected with approximately 96.0% confidence.
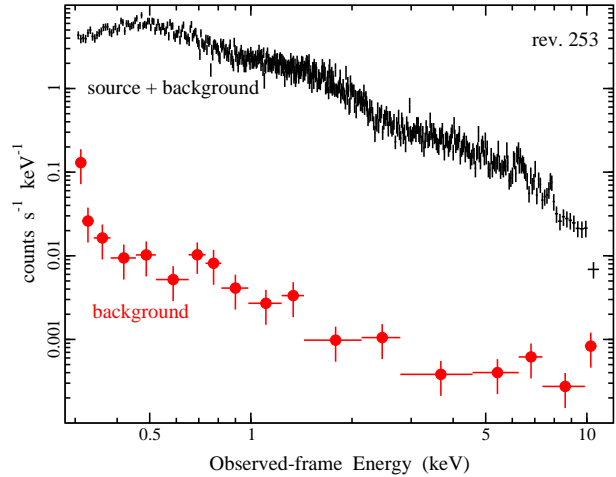
Figure 2. The top curve of data points (black crosses) represent the source plus background pn spectrum during observation 253. The lower curve (red dots) is the background pn spectrum extracted from a source-free region and scaled to the source plus background extraction region.

3.3 Sanity checks

3.3.1 *Background contamination and instrumental emission lines*

As the observations were conducted in small window mode and with short exposures the background level is very low. During both observations, UGC 3973 was significantly detected above the background level (Figure 2). The total number of source plus background counts collected by the pn instrument in the $7 - 10 \, \mathrm{keV}$ range during revolution 253 was 413. In comparison, only 8 background counts were collected in the $7 - 10 \, \mathrm{keV}$ range from an extraction region of the same size as the source cell.

To understand the background emission produced by the pn detector Freyberg et al. (2004) analysed $313 \, \mathrm{ks}$ of data obtained in closed filter position during the first three years of operations. In doing so they accurately determined the spatial and temporal behaviour of background spectral features. The background features most relevant to our analysis are the emission lines from Ni Kα ($E = 7.48 \, \mathrm{keV}$) and Cu Kα ($E = 8.05 \, \mathrm{keV}$). These lines originate from the electronics board mounted below the CCD and they are spatial inhomogeneous across the camera. Emission is weakest in the centre of the detector (close to the on-axis position) which is located above the venting hole in the circuit board (see figure 4 of Freyberg et al.). When the pn detector is operated in nominal small window mode, as was the case for both observations of UGC 3973, the exposed part of the CCD is located above the venting hole and contamination from Ni and Cu is minimised.

Furthermore, and more importantly, the $8 \, \mathrm{keV}$ (rest frame) emission line is found at $\sim 7.8 \, \mathrm{keV}$ in the observed frame. The energy is formally inconsistent with any background emission features at greater than 3σ (Figure 3). The combination of the low background level, observed energy of the feature, and the minimal contamination expected from background lines in small window mode, makes it very unlikely that the feature could arise from instrumental effects.
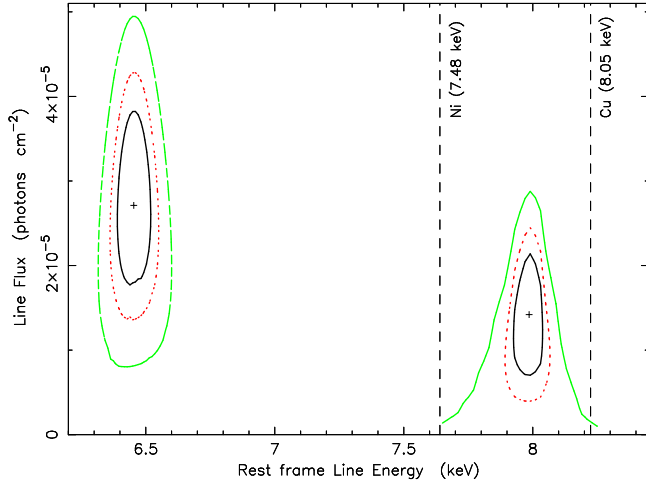
Figure 3. The plot show the 1, 2, and 3σ confidence levels (line flux as a function of rest frame line energy) from fitting a Gaussian profile at $\sim$ $6.45\,\mathrm{keV}$ and another at $\sim 7.99\,\mathrm{keV}$. The vertical dashed lines mark the energies (shifted to the source frame) of the background emission lines (Cu and Ni) in the region around the $\sim 7.99\,\mathrm{keV}$ feature.

3.3.2   MOS spectra

The broadband spectral modelling of the MOS data are in good agreement with the pn results; however the $\sim 8\,\mathrm{keV}$ feature is not detected. Simulations were conducted to examine if the null detection could be a consequence of the lower sensitivity of the MOS cameras at $8\,\mathrm{keV}$ compared to the pn. To the best fitting model obtained with the MOS data a Gaussian profile was added with the parameters (energy, width, and normalisation) as measured from the pn data. The MOS observations from revolution 253 were then simulated. The residuals resulting from fitting a power-law to the $2.5 - 10\,\mathrm{keV}$ simulated spectra are shown in Figure 4. An emission line is not detected in the simulated MOS observations indicating that the absence of an $8\,\mathrm{keV}$ feature in the MOS is most likely a sensitivity issue.

### 3.4   Is the feature transient?

3.4.1   Long-term variability

The question as to whether the $8\,\mathrm{keV}$ feature is variable or transient is of fundamental importance in determining its origin. Approximately six months earlier during the first observation (rev. 153) there was no significant detection of a feature around $8\,\mathrm{keV}$. When fixing a Gaussian profile at $8\,\mathrm{keV}$ with the same parameters as found during revolutions 253, we determine the 90% upper-limit on the line flux to be $1.57 \times 10^{-13}\,\mathrm{erg\,cm^{-2}\,s^{-1}}$, which is still consistent with the 90% confidence levels reported for the flux of the $8\,\mathrm{keV}$ feature during revolution 253 (Section 3.1).

The continuum flux of UGC 3973 during revolution 153 was twice as high compared to revolution 253, and this could possibly explain the absence of a firm detection of the line during the first observation. To clarify the situation, a simulation of the pn observation during revolution 153 was carried out. To the best-fit broadband model measured during revolution 153 a Gaussian profile was included, with the same parameters as measured during revolution 253. In addition to the higher continuum flux, the high-energy spectrum is also steeper during revolution 153. Consequently, a *constant-flux* emission line should have been detectable with about the same strength and significance as found at the later
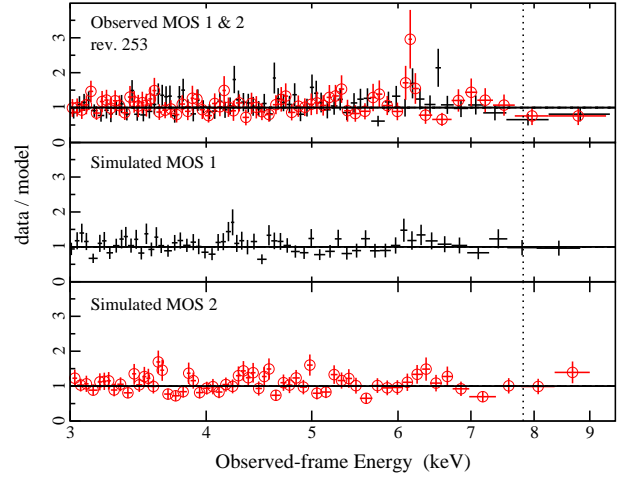

Figure 4. In the top panel are the observed MOS 1 (black crosses) and MOS 2 (red open circles) residuals (data/model) remaining after fitting the $2.5 - 10\,\mathrm{keV}$ data from revolution 253 with a power-law. There is no detection of a $\sim 8\,\mathrm{keV}$ feature (marked by the dotted vertical line) as seen in the pn. The residuals shown in the middle and lower panels result from fitting a power-law to simulations of the MOS observations (from rev. 253) which include an $\sim 8\,\mathrm{keV}$ feature as found in the pn. There are no indications of an $\sim 8\,\mathrm{keV}$ emission line in the simulated observations. The lack of a MOS detection appears to be a sensitivity issue.
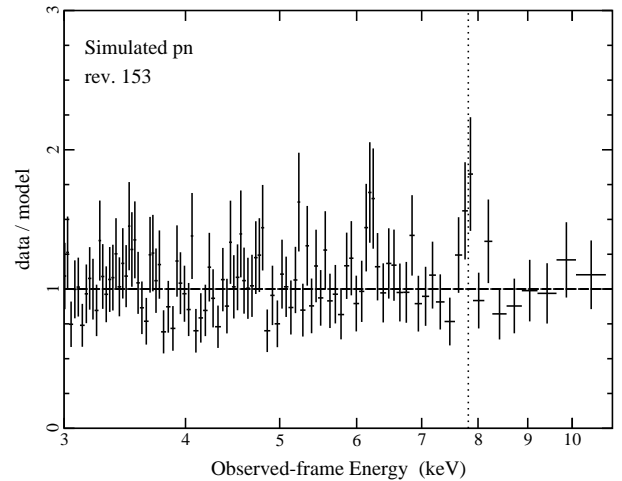
Figure 5. A simulation of the pn spectrum from revolution 153 including an $\sim 8\,\mathrm{keV}$ emission line with the same flux as measured during revolution 253 (marked by the dotted vertical line) Assuming the line flux remained constant, the emission line should have been detected during revolution 153 despite the continuum being twice as bright.

epoch (Figure 5). The addition of a Gaussian profile with three free parameters (energy, width, and normalisation) to the broadband simulated spectrum improves the fit by $\Delta\chi^2 = 8.6$.

This suggests that the $8\,\mathrm{keV}$ feature may be variable or transient, but we can not completely exclude the possibility of a constant-flux emission line.
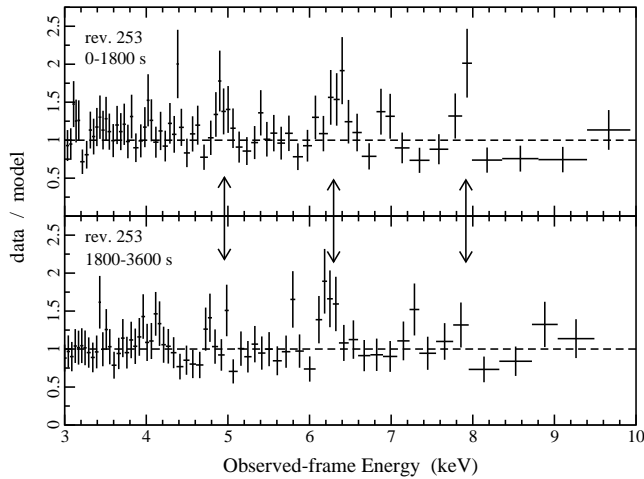
Figure 6. The ratio resulting from fitting a power-law to the $2.5 - 10 \, \text{keV}$ pn band during two different intervals of revolution 253. The spectrum from the first half of the observation ($< 1800 \, \text{s}$) is shown in the top panel. In the lower panel, the spectrum from the second half ($> 1800 \, \text{s}$) of the observation is displayed. Three double-headed arrows mark the possible line emission at about 5, 6.4, and 8 keV. All three features are visible in the first half of the observation, but only the $\sim 6.4 \, \text{keV}$ line is present in the second half.

3.4.2 Rapid variability

Due to the very low background during the observation it is possible to examine short-term variability in the spectrum. Over the course of the $\sim 3600 \, \text{s}$ exposure (revolution 253) light curves of UGC 3973 are consistent with a constant and there is no change in the broadband continuum flux. In order to examine possible variability in the features themselves, the spectrum from revolution 253 was divided into two halves each containing about $1800 \, \text{s}$ of data. The $2.5 - 10 \, \text{keV}$ spectra from both intervals were then fitted with a power-law, the ratios of which are shown in Figure 6.

During both intervals the $\sim 6.4 \, \text{keV}$ line is present with approximately the same strength and flux (Table 3). Interestingly, the $\sim 8 \, \text{keV}$ feature is significantly detected only in the first interval. Moreover, there is another narrow spectral feature at $\sim 5 \, \text{keV}$, which is also only detected during the first half of the observation.

During the second interval only the $\sim 6.4 \, \text{keV}$ emission line is statistically required. If we fix a Gaussian profile at $5 \, \text{keV}$ and another at $8 \, \text{keV}$ and fit the data from the second interval, we notice that both lines have decreased in strength by about the same amount ($\Delta EW \approx -110 \, \text{eV}$). Meanwhile, the strength and flux of the $\sim 6.4 \, \text{keV}$ emission line, and the continuum flux and photon index remain constant throughout the observation (Table 3). However, the changes in the 5 and 8 keV features are trends as opposed to significant variations since, within 90% confidence levels, only the equivalent width of the $5 \, \text{keV}$ feature is different.

These possible variations suggest that if both line-like features are real they may be related in such a way that they vary simultaneously. Since the features are only observed for the first half of the observation it is impossible to estimate how long they were present in the spectrum prior to the onset of the observation. The high-energy spectral fit parameters for each of the two intervals are shown in Table 3.

4 DISCUSSION

There are several reports of emission lines at energies inconsistent with iron emission. These features tend to be redshifted to energies between $5 - 6 \, \text{keV}$ (e.g. Turner et al. 2002, 2004; Porquet et al. 2004), and reports of blueshifted emission features are few. Extreme blueshifts, on the order of $\sim 0.7c$ have been reported in two objects (Yaqoob et al. 1999; Wang et al. 2003). Both these sources are radio-loud, thus a mechanism to launch material at such velocities can be envisaged. Another blueshifted line was reported at $7.6 \, \text{keV}$ in a radio-quiet, narrow-line Seyfert 1 galaxy (Ghosh et al. 2004). There are some possible physical explanation as to why there are more reports of redshifted features than blueshifted ones, though it could simply be that the sensitivity of current X-ray instruments (i.e. *XMM-Newton* and *Chandra*) drops quickly at energies above $\sim 7 \, \text{keV}$.

4.1 Atomic transitions

4.1.1 Emission lines

From the CHIANTI v4.2 database (Dere et al. 1997; Young et al. 2003), we find that an atomic transition arising around $8 \, \text{keV}$ originates from H-like Ni ($E = 8.0730 \, \text{keV}$). In the time-averaged spectrum (reported in Table 2) the best-fit line energy is formally inconsistent with Ni at more than 3σ. However, in the first half of the split spectrum (Table 3) the measured line energy is comparable with Ni XXVIII. This raises a second problem in that an extraordinary abundance of nickel is required to produce such a strong line. Assuming solar abundances for iron (Anders & Grevesse 1989), we estimate that a minimum nickel overabundance of $\sim 15\times$ solar is necessary to account for the average flux of the $\sim 8 \, \text{keV}$ feature over the duration of the observation.

Gastaldello & Molendi (2004) suggested an overabundance of nickel, probably due to enrichment from SN Ia (Dupke & Arnaud 2001), to explain the excess flux between $7 - 8 \, \text{keV}$ in the spectrum of the Perseus cluster. This scenario does not seem valid for UGC 3973 for a number of reasons. Firstly, the overabundance is quite extreme ($> 15\times$ solar). Secondly, the $\sim 8 \, \text{keV}$ in UGC 3973 appears to be variable on various time scales. Flux variations would not be noticed from supernova emission unless there was bulk motion of ejecta, which is at odds with the narrowness of the measured feature. Of course, we cannot completely rule out that the environment was enriched at an earlier epoch, and now the variability is due to accretion processes. Thirdly, though not a necessary condition, a Ni overabundance does not explain the possible detection of the variable $\sim 5 \, \text{keV}$ emission line.

4.1.2 Radiative recombination edges

Radiative recombination edge and continuum (RRC) of ionised iron can result in line-like features above $7 \, \text{keV}$, specifically $9.28 \, \text{keV}$ and $8.83 \, \text{keV}$ for H- and He-like iron, respectively. The width of the feature reveals the characteristic electron temperature (kT_e). For a photoionised plasma the electron temperature can be significantly less than the ionisation potential; thus the RRC feature can appear quite narrow (see reviews by Liedahl 1999; Kahn et al. 2002). Radiative recombination features have been proposed to describe the X-ray afterglow spectra of some gamma-ray bursts (e.g. Yoshida et al. 2002; Piro et al. 2000).

The $8 \, \text{keV}$ feature in UGC 3973 can be well fitted with a RRC ($\chi^2_\nu/\text{dof} = 1.00/501$) with a plasma temperature of $kT_e < 140 \, \text{eV}$.

Table 3. High-energy spectral features at two $1800\,\mathrm{s}$ intervals during revolution 253. Column (1): interval exposure. Column (2) is the power-law normalisation in units of $10^{-3}\,\mathrm{photons\,keV^{-1}\,cm^{-2}\,s^{-1}}$ at $1\,\mathrm{keV}$. Columns (3) shows the rest frame of the line feature. Column (4) marks the fit improvement achieved by adding the component to the fit from the row above. Columns (5), (6), and (7) are the width, equivalent width and flux of each respective line feature. Values marked with an f denote fixed parameters.

| (1) Time Interval (s)	(2) n	(3) E (keV)	(4) $\Delta\chi^2$	(5) σ (eV)	(6) EW (eV)	(7) f_l ($10^{-13}\,\mathrm{erg\,cm^{-2}\,s^{-1}}$)
$0-1800$	$2.48^{+0.47}_{-0.39}$	$6.48^{+0.07}_{-0.10}$		<220	229^{+189}_{-131}	$2.87^{+2.21}_{-1.55}$
		8.05 ± 0.06	$5.3/2$	1^f	212^{+113}_{-93}	$2.37^{+1.69}_{-1.51}$
		5.03 ± 0.06	$9.6/2$	1^f	117^{+64}_{-66}	$1.72^{+0.83}_{-0.99}$
$1800-3600$	$2.54^{+0.58}_{-0.40}$	$6.38^{+0.07}_{-0.06}$		<130	198^{+164}_{-98}	$2.44^{+1.42}_{-1.21}$
		8^f	$1.7/1$	1^f	97^{+83}_{-71}	<2.39
		5^f	$0.2/1$	1^f	9^{+38}_{-9}	<0.86

The observed threshold energy (taking into consideration the host-galaxy redshift) would require an outflowing velocity of approximately 0.14 or $0.10\,c$, depending on the ionisation state of iron. The RRC should also be accompanied by a redshifted, ionised, emission line. Unfortunately, the redshifted emission line, regardless of the ionisation, should appear close to, or within, the neutral Fe $K\alpha$ feature observed between $6-6.5\,\mathrm{keV}$; thus it is not possible to derive any meaningful limits on a redshifted, ionised line component.

4.2 Relativistic disc line and orbiting hot spots

There are a number of examples (e.g. Della Ceca et al. 2005, and references within) where narrow emission features have been attributed to the "horns" of the disc line profile (Fabian et al. 1989). Our attempt to model the feature with a disc line profile resulted in a good fit ($\chi^2_\nu/\mathrm{dof} = 1.01/502$; Figure 7). The energy of the disc line was fixed to $6.7\,\mathrm{keV}$ as allowing it to remain free did not enhance the fit. The equivalent width was $EW \approx 400\,\mathrm{eV}$. Emission was assumed to be coming from a thin ring between $15-15.5\,r_\mathrm{g}$ ($r_\mathrm{g} = GM/c^2$). The derived disc inclination ($i = 60^{+6}_{-3}$ degrees) is consistent with the optical classification of UGC 3973 as a Seyfert 1.2 (Pietsch et al. 1998). The horns of the disc line profile are observed at ~ 7.8 and $4.9\,\mathrm{keV}$ (observed frame), which accurately correspond to the energies of the $8\,\mathrm{keV}$ feature under investigation, as well as the slight excess at $\sim 5\,\mathrm{keV}$ seen in Figure 6.

Assuming a $\sim 6\times10^7\,\mathrm{M_\odot}$ black hole, implies that the radiation only needs to flash briefly ($15\,r_\mathrm{g}/c \approx 4500\,\mathrm{s}$). This is on the same order as the lower-limit established from the apparent variability of the lines in Figure 6. The effect could be of radiation propagating from the centre shining on an irregularity in disc height, perhaps an inflowing lump or some sort of ridge in the disc.

Localised hot spots which illuminate a small portion of the disc (e.g. Dovčiak et al. 2004) could also produce such a narrow feature at $8\,\mathrm{keV}$. The possible $5\,\mathrm{keV}$ line seen in Figure 6 appears as though it could be displaying similar variability as the $8\,\mathrm{keV}$ line. If we insist on connecting the behaviour of these two features (which we do not), then it would be challenging to describe both of them as arising under the same physical conditions in the hot spot model.
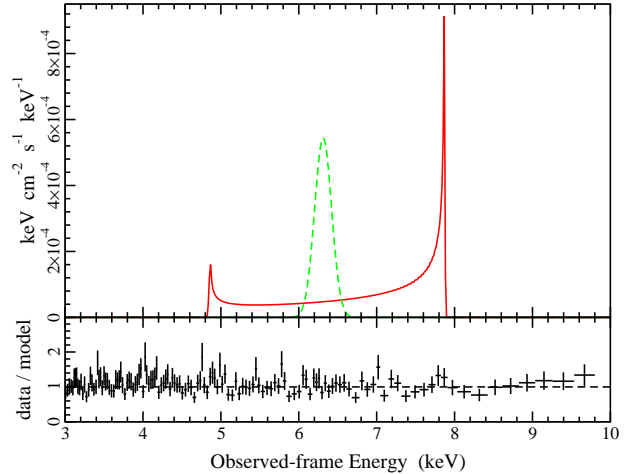
Figure 7. Upper panel: The emission line profiles used to fit the near-neutral iron emission and the narrow feature at $8\,\mathrm{keV}$. The red solid line is the disc line profile as described in the text, and the green dashed line is the Gaussian profile used to fit the $\sim 6.4\,\mathrm{keV}$ emission line. The red horn of the disc line profile is at about $4.9\,\mathrm{keV}$ which could describe the residuals seen at that energy in the top panel of Figure 6. Lower panel: The residuals (data/model) remaining in the $3-10\,\mathrm{keV}$ band after applying a power-law plus the two line profiles shown in the upper panel to the pn data of UGC 3973 during rev. 253.

4.3 Outflows

Both red and blueshifted *absorption* features have been reported in radio-quiet AGN (e.g. Nandra et al. 1999; Matt et al. 2005; Dadina et al. 2005), and the aborted jet scenario (Ghisellini et al. 2004) works well at describing them.

In principle the aborted jet scenario can also describe emission features, but this would imply that the line is being emitted at a large distance from the central region. If attributed to blueshifted iron, the $\sim 8\,\mathrm{keV}$ emission line in UGC 3973 requires a outflowing velocity between $0.15-0.25\,c$ (depending on the ionisation state of iron). The high velocity measured in the X-rays is inconsistent with velocities seen at other wavelengths.

If we once again suppose that the $8\,\mathrm{keV}$ and $5\,\mathrm{keV}$ features are interconnected we can speculate that both are originating from slightly ionised iron ($E = 6.5\,\mathrm{keV}$), and moving in opposite di-

rections, but with the same speed ($\approx 0.2\ c$). The slightly weaker $5\,\mathrm{keV}$ line would be consistent with suppressed emission from matter moving away from the observer. Such a condition could arise in a jet outflow, for example from material which is ejected in both directions at the same time. Such a twin-jet scenario involving emission lines is not unprecedented and has been proposed for the Galactic binary SS 433 (e.g. Fabian & Rees 1979; see Brinkmann et al. 2005 for recent X-ray spectra).

5 CONCLUSIONS

We presented the analysis of an $8\,\mathrm{keV}$ emission line feature in the Seyfert 1.2, UGC 3973. We have intensely scrutinised the detection and determine that the feature is significant at a confidence level between $96.0 - 98.4\%$, depending on what a priori assumptions are made. The fact that the feature is blue shifted with respect to iron emission is intriguing. However, since the exposure was so short ($< 3600\,\mathrm{s}$) it is not possible to draw substantial conclusions. The brightness and complexity of the feature make UGC 3973 a worthy target for follow-up observations with *XMM-Newton*, *Chandra*, *Astro-E 2*, and in the future *XEUS*.

REFERENCES

Anders E., Grevesse N., 1989, GeCoA, 53, 197

Arnaud K., 1996, in: *Astronomical Data Analysis Software and Systems*, Jacoby G., Barnes J., eds, ASP Conf. Series Vol. 101, p17

Brinkmann W., Kotani T., Kawai N., 2005, A&A, 431, 575

Dadina M., Cappi M., Malaguti G., Ponti G., De Rosa A., 2005, accepted by A&A (astro-ph/0506697)

Della Ceca R., Ballo L., Braito V., Maccacaro T., 2005, accepted by ApJ, (astro-ph/0503665)

Dere K., Landi E., Mason H., Monsignori Fossi B., Young P., 1997, A&AS, 125

Dickey J. M., Lockman F. J., 1990, ARA&A, 28, 215

Dovčiak M., Bianchi S., Guainazzi M., Karas V., Matt G., 2004, MNRAS, 350, 745

Dupke R., Arnaud K., 2001, ApJ, 548, 141

Fabian A. C., Rees M. J., 1979, MNRAS, 187, 13

Fabian A. C., Rees M. J., Stella L., White N. E., 1989, MNRAS, 238, 729

Freyberg M. J. et al. 2004, in Flanagan K., Siegmund O., eds, *X-Ray and Gamma-Ray Instrumentation for Astronomy XIII*, Proceedings of the SPIE, 5165, 112

Gallo L., Lehmann I., Pietsch W., Boller T., Brinkmann W., Friedrich P., Grupe D., 2005, submitted to MNRAS (G05)

Gastaldello F., Molendi S., 2004, ApJ, 600, 670

Ghisellini G., Haardt F., Matt G., 2004, A&A, 413, 535

Ghosh K., Swartz D., Tennant A., Wu K., Ramsey B., 2004, ApJ, 607, 111

Ho L., 2002, ApJ, 564, 120

Jansen F. et al. 2001, A&A, 365, L1

Kahn S., Behar E., Kinkhabwala A., Savin D., 2002, RSPTA, 360, 1923

Liedahl D., 1999, LNP, 520, 189

Matt G., Porquet D., Bianchi S., Falocco S., Maiolino R., Reeves J., Zappacosta L., 2005, Accepted by A&A, (astro-ph/0502323)

Nandra K., George I., Mushotzky R., Turner T., Yaqoob T., 1999, ApJ, 523, 17

Peterson B. et al. 2004, ApJ, 613, 682

Pietsch W., Bischoff K., Boller Th., Döbereiner S., Kollatschny W., Zimmermann H.-U., 1998, A&A, 333, 48

Piro L. et al. 2000, Sci, 290, 955

Porquet D., Reeves J, Uttley P., Turner T. J., 2004, A&A, 427, 101

Strüder L. et al. 2001, A&A, 365, L18

Turner M. J. L. et al. 2001, A&A, 365, 27

Turner T. J. et al. 2002, ApJ, 574, L123

Turner T. J., Kraemer S. B., Reeves J. N., 2004, ApJ, 603, 62

Vestergaard M., 2002, ApJ, 571, 733

Wandel A., Peterson B., Malkan M., 1999, ApJ, 526, 579

Wang J. et al. 2003, ApJ, 590, 87

Yaqoob T., George I. M., Nandra K,; Turner T., Zobair S., Serlemitsos J., 1999, ApJ, 525, 9

Yoshida A. et al. 2001, ApJ, 557, 27

Young P., Del Zanna G., Landi E., Dere K., Mason H., Landini M., 2003, ApJS, 144

This paper has been typeset from a TEX/ LATEX file prepared by the author.